POLITECNICO DI TORINO
Repository ISTITUZIONALE

Hybrid injectable platforms for the in situ delivery of therapeutic ions from mesoporous glasses

Original
Hybrid injectable platforms for the in situ delivery of therapeutic ions from mesoporous glasses / Pontremoli, C.; Boffito, M.; Fiorilli, S.; Laurano, R.; Torchio, A.; Bari, A.; Tonda-Turo, C.; Ciardelli, G.; Vitale-Brovarone, C.. - In: CHEMICAL ENGINEERING JOURNAL. - ISSN 1385-8947. - ELETTRONICO. - 340:(2018), pp. 103-113. [10.1016/j.cej.2018.01.073]

Availability:
This version is available at: 11583/2701310 since: 2018-03-22T17:14:38Z

Publisher:
Elsevier

Published
DOI:10.1016/j.cej.2018.01.073

Terms of use:

This article is made available under terms and conditions as specified in the corresponding bibliographic description in the repository

Publisher copyright

(Article begins on next page)

12 October 2024

Chemical Engineering Journal 340 (2018) 103–113

Contents lists available at ScienceDirect

Chemical Engineering Journal

journal homepage: www.elsevier.com/locate/cej

Hybrid injectable platforms for the in situ delivery of therapeutic ions from mesoporous glasses

C. Pontremoli[a,1], M. Boffito[b,1], S. Fiorilli[a,*], R. Laurano[b], A. Torchio[b], A. Bari[a], C. Tonda-Turo[b], G. Ciardelli[b], C. Vitale-Brovarone[a]

[a] Department of Applied Science and Technology, Politecnico di Torino, Corso Duca degli Abruzzi 24, 10129 Torino, Italy
[b] Department of Mechanical and Aerospace Engineering, Politecnico di Torino, Corso Duca degli Abruzzi 24, 10129 Torino, Italy

HIGHLIGHTS

- Cu-containing MBGs (Cu-MBG) synthesised as micro and nanospheres.
- Cu-MBGs incorporated into an injectable polyurethane hydrogel.
- Sustained and prolonged release of Cu^{2+} ions from incorporated Cu-MBGs.
- Hybrid injectable formulations for *in situ* delivery of therapeutic ions.

GRAPHICAL ABSTRACT

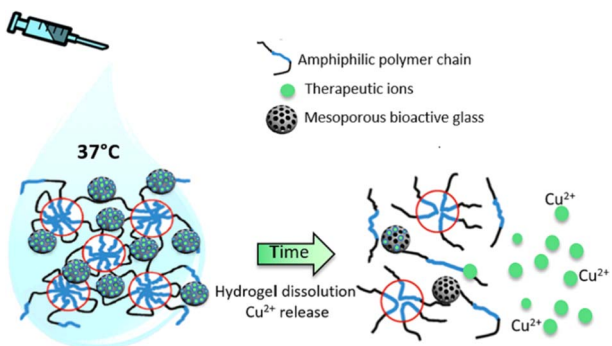

ARTICLE INFO

Keywords:
Mesoporous bioactive glasses
Copper
Polyurethane
Injectable hydrogels
Thermosensitivity

ABSTRACT

Copper-containing bioactive glasses (Cu-MBGs) are attracting increasing interest as multifunctional agents for hard and soft tissue healing due to the ability of released copper ions to stimulate osteogenesis as well as angiogenesis and to impart anti-bacterial properties. The conjugation of these nanomaterials with a vehicle phase based on thermosensitive hydrogels represents an effective strategy to design non-invasive injectable devices for the *in situ* delivery of therapeutic ions from MBGs.

In this contribution, Cu-containing MBGs were prepared by an aerosol-assisted spray-drying method (MBG_Cu 2%_SD) in the form of microspheres (surface area of *ca* 220 $m^2 g^{-1}$) and through a sol-gel synthesis (MBG_Cu 2% _SG) in the form of spheroidal nanoparticles (surface area above 700 $m^2 g^{-1}$). Both Cu-containing samples were able to release copper ions, although with different rates and percentage release. MBG_Cu 2%_SG released the total incorporated amount of Cu ions with a faster kinetics compared to MBG_Cu 2%_SD, that released approximately the 60% of copper.

Cu-MBGs were incorporated with a final concentration of 20 mg/mL into a thermosensitive sol-gel system consisting of a novel amphiphilic poly(ether urethane) based on a commercialy available Poloxamer 407 (P407), with improved gelation ability, mechanical strength and stability in aqueous solution with respect to native P407. Cu-MBG-loaded hydrogels were characterised in terms of sol-to-gel transition temperature and time, injectability and stability in aqueous environment at 37 °C. The hybrid formulations showed fast gelation in physiological conditions (1 mL underwent complete sol-to-gel transition within 3–5 min at 37 °C) and injectability in a wide range of temperatures (5–37 °C) through different needles (inner diameter in the range 0.6–1.6 mm).

* Corresponding author.
E-mail address: sonia.fiorilli@polito.it (S. Fiorilli).
[1] Equal contribution.

https://doi.org/10.1016/j.cej.2018.01.073

Available online 16 January 2018
1385-8947/ © 2018 The Authors. Published by Elsevier B.V. This is an open access article under the CC BY-NC-ND license (http://creativecommons.org/licenses/BY-NC-ND/4.0/).

When embedded into the hydrogel, Cu-MBGs retained their release properties, showing a sustained delivery of Cu^{2+} along 14 days.

1. Introduction

The use of organized mesoporous materials continues to gain interest in a wide range of biomedical applications due to their ability to store and release drugs/biomolecules and to the possibility to impart stimuli-responsive and/or targeting properties through surface functionalization [1–3].

In the field of advanced bioceramics, templated mesoporous glasses, which combine the textural features of ordered mesoporous matrices, i.e. very high exposed surface area and pore volume, with the properties of conventional bioactive sol-gel glasses, have shown excellent behaviour as systems for bone-tissue regeneration [4–6]. More recently, with the aim to develop a smart and versatile technology platform for highly targeted therapies for pathological tissues (hard and soft), the composition of mesoporous bioactive glasses (MBGs), conventionally synthesized in the systems SiO_2-CaO or SiO_2-CaO-P_2O_5, has been enriched with controlled amount of therapeutic elements, as Ag^+, Sr^{2+}, Cu^{2+} and Co^{2+}, whose release is able to impart specific biological functions, including anti-bacterial activity, as well as stimulation of osteogenesis and angiogenesis [7–11]. In particular, several studies have extensively proven the ability of released copper ions to enhance bone regeneration and vascularization, as well as wound healing [12,13]. Very recently, Wu and co-workers finely demonstrated the role of Cu^{2+} ions released from mesoporous silica nanospheres in inducing osteogenic/angiogenic response while suppressing osteo-clastogenic activity [14]. The sustained release of copper ions from MBGs can also act as an effective anti-microbial agent against both bacterial growth and biofilm formation/dispersion, providing a true alternative to traditional antibiotic systemic therapies [15]. Furthermore, the release of therapeutic ions can be synergistically combined with the delivery of pharmaceutical agents or growth factors incorporated into the internal cavities or adsorbed/grafted on the external surface.

The resulting multifunctional nanocarriers are ideal candidates for the development of novel clinical devices able to simultaneously target all the causes, often mutually interlocked, leading to compromised tissue healing. To this aim, the conjugation of these carriers with a vehicle phase based on thermosensitive hydrogels, in which an aqueous solution undergoes a sol to gel transition in physiological conditions (37 °C), represents an effective strategy to design non-invasive devices that can be injected into the pathological site and, after gelling *in situ*, will result in an ion/drug depot for prolonged and localised release. Recently, the feasibility of this approach has been proven for the preparation of an anticancer depot system based on thermosensitive Pluronic F127 hydrogel carrying doxorubicin-loaded mesoporous silica nanoparticles [16]. Pluronic F127, also coded as Poloxamer 407, is a poly(ethylene oxide)-poly(propylene oxide)-poly(ethylene oxide) (PEO-PPO-PEO) triblock copolymer extensively used in biomedical applications [17]. However, Pluronic F127-based hydrogels suffer of poor stability in aqueous environment, starting to dissolve few minutes after injection and thus do not allow a prolonged and sustained release overtime [18,19]. One of the most commonly investigated approaches to overcome this limitation consists in chain extending Pluronic F127 through the chemistry of polyurethanes (PURs), which, amongst other things, also allows the introduction of specific moieties for further functionalization, targeted degradation or specific cell behaviour along the polymer backbone. As a consequence of the high chemical versatility that characterizes this class of polymeric materials, a wide range of PUR compositions has been designed and thoroughly investigated for different applications in the fields of regenerative medicine and pharmaceutics, ranging from implantable biostable devices to biodegradable scaffolds and delivery systems [18–27]. Hence, PURs act as a flexible platform of materials able to fit the requirements imposed by the final application. In particular, PUR composition can be opportunely selected based on the required mechanical properties of the resulting PUR-based device: rigid polyurethane scaffolds are suitable for bone tissue replacement [28–30], while soft polyurethane constructs better fit with the regeneration of soft tissues (i.e. cardiac, vascular and nerve tissues) [25,31,32].

For some applications, such as filling of restricted, non load bearing defect sites, injectable PUR-based hydrogels, able to perfectly take the shape of the defect cavity prior to their complete gelation, have been successfully developed to allow easy administration and minimally invasive injection [33].

In this regard, Boffito et al. [18] recently reported the synthesis of a novel amphiphilic poly(ether urethane) (PEU) based on Poloxamer 407, with improved gelation ability, mechanical strength and stability compared to the commercially available Poloxamer 407, showing promising features for application in tissue engineering/regenerative medicine and drug release as *in situ* injectable delivery systems. In the literature, injectable PURs developed for bone tissue engineering have been conjugated with an inorganic phase, such as tricalcium phosphate or mineralized bone particles, with the aim to improve the mechanical properties and confer osteoconductivity to the final hybrid constructs [31,34].

In this study, with the aim to prepare an injectable hybrid formulation able to release *in situ* therapeutic ions from MBG particles, a Poloxamer 407-based PEU has been synthesized according to a previously published method [20] and its aqueous solutions have been loaded with MBGs belonging to the SiO_2-CaO-CuO system to design a hybrid thermosensitive MBG-PEU platform.

Copper-containing MBGs have been prepared in the form of micro- and nano-spheres by following two synthesis approaches in order to evaluate the effect of particle size and size distribution on the resulting formulation properties. The obtained MBG-PEU systems have been investigated in terms of sol-to-gel transition temperatures and time, injectability and stability in aqueous environment at 37 °C to mimic the real working conditions of the developed systems. The release profiles of Cu^{2+} ions from the glass matrices alone and upon loading into the hydrogel have been assessed and the obtained kinetics compared.

2. Materials and methods

2.1. Preparation of Cu-containing MBGs

Copper-loaded MBGs were prepared through two different synthesis approaches in order to obtain particles with different size and structural parameters (i.e. specific surface area, pore size).

2.1.1. Preparation of Cu-containing MBG nanoparticles by sol-gel synthesis

The first procedure is a base-catalysed sol-gel synthesis, as reported by Wu et al. [35] to produce mesoporous calcium-silicate nanoparticles, where copper replaces part of calcium. In particular, MBG with 2% molar percentage of Cu (molar ratio Cu/Ca/Si = 2/13/85, named hereafter as MBG_Cu 2%_SG) was prepared as follows: 6.6 g cetyltrimethylammonium bromide (CTAB ≥ 98%, Sigma Aldrich, Italy) and 12 mL NH_4OH (Ammonium hydroxide solution, Sigma Aldrich, Italy) were dissolved in 600 mL of double distilled water (ddH_2O) under stirring for 30 min. Then, 30 mL tetraethyl orthosilicate (TEOS, Tetraethyl orthosilicate, Sigma Aldrich, Italy), 4.888 g of calcium nitrate tetrahydrate ($Ca(NO_3)_2{\cdot}4H_2O$, 99%, Sigma Aldrich, Italy) and 0.428 g of

copper chloride ($CuCl_2$ 99%, Sigma Aldrich, Italy) were added under vigorous stirring for 3 h. The powder was collected by centrifugation (Hermle Labortechnik Z326) at 10,000 rpm for 5 min, washed one time with distilled water and two times with absolute ethanol. The final precipitate was dried at 70 °C for 12 h and calcined at 600 °C in air for 5 h at a heating rate of 1 °C min^{-1} using a Carbolite 1300 CWF 15/5, in order to remove remaining traces of CTAB.

2.1.2. Preparation of Cu-containing MBG microspheres by aerosol-spray-assisted approach

MBG microspheres with 2% molar percentage of Cu (molar ratio Cu/Ca/Si = 2/13/85, hereafter named as MBG_Cu 2%_SD) were synthesized by modifying a spray-drying method reported by Pontiroli et al. [36]. Briefly, 2.030 g of the non-ionic block copolymer Pluronic P123 ($EO_{20}PO_{70}EO_{20}$, average M_n ~5800 Da, Sigma Aldrich, Italy) were dissolved in 85 g of ddH_2O. In a separate batch, a solution of 10.73 g of TEOS was pre-hydrolysed under acidic conditions using 5 g of an aqueous HCl solution at pH 2 until a transparent solution was obtained. The solution with TEOS was then poured drop by drop into the template solution and kept stirring for 1 h. Then, 0.163 g of copper chloride ($CuCl_2$ 99%, Sigma Aldrich, Italy) and 1.86 g of calcium nitrate tetrahydrate ($Ca(NO_3)_2$ $4H_2O$, 99%, Sigma Aldrich, Italy) were added.

The final solution was stirred for 15 min and then sprayed (Büchi, Mini Spray-Dryer B-290) using nitrogen as the atomizing gas with the following parameters: inlet temperature 220 °C, N_2 pressure 60 mmHg and feed rate 5 mL/min. The obtained powder was finally calcined at 600 °C in air for 5 h at a heating rate of 1 °C min^{-1} using a Carbolite 1300 CWF 15/5.

2.2. Cu-containing MBG characterization

2.2.1. Physico-chemical characterization of Cu-MBGs

The morphology of MBG particles was analyzed by Field-Emission Scanning Electron Microscopy (FE-SEM) using a ZEISS MERLIN instrument. For FE-SEM observations, 10 mg of MBG_Cu 2%_SG powder was dispersed in 10 mL of isopropanol using an ultrasonic bath (Digitec DT 103H, Bandelin) for 5 min to obtain a stable suspension. 5 µL of the resulting suspension was dropped on a carbon coated copper grid (3.05 mm Diam.200 MESH, TAAB) and successively coated with Cr layer for FE-SEM and EDS mapping analysis.

MBG_Cu 2%_SD powder was dispersed on a conductive carbon tape and coated with Cr layer. Compositional analysis of the powders was performed by energy dispersive spectroscopy (EDS; AZtec EDS, Oxford instruments).

EDS spectra were collected on powders dispersed on carbon tape by analysing an area of 75 × 50 µm. The samples were characterized by wide-angle (2ϑ within 10–80°) X-ray diffraction (XRD, X'Pert PRO, PANalytical). Nitrogen adsorption-desorption isotherms were measured at -196 °C using an ASAP2020, Micromeritics. Samples were outgassed at 150 °C for 5 h before analysis. The Brunauer-Emmett-Teller (BET) equation was used to calculate the specific surface area (SSA_{BET}) from the adsorption data (relative pressures 0.04–0.2). The pore size distribution was evaluated through the DFT method (Density Functional Theory) using the NLDFT kernel of equilibrium isotherms (desorption branch).

2.2.2. In vitro bioactivity test

Cu-containing MBG bioactivity was assessed by soaking 30 mg in 30 mL of simulated body fluid (SBF), as reported in the literature [37]. The samples were kept immersed at 37 °C up to 14 days, inside an orbital shaker Excella E24, Eppendorf, with an agitation rate of 150 rpm. At each time point (1 day, 7 days and 14 days) the powders were separated by centrifugation at 5000 rpm for 5 min, washed with distilled water and dried in oven at 70° C for 12 h. Hydroxyapatite formation was assessed by FESEM/EDS and wide-angle (2ϑ within 10–80°) X-ray diffraction (XRD, X'Pert PRO, PANalytical).

2.2.3. Evaluation of Cu ion release from Cu-containing MBG particles

In order to evaluate Cu ion release, MBG_Cu 2%_SG and MBG_Cu 2%_SD samples were suspended in Tris HCl buffer (Tris(hydroxymethyl) aminomethane (Trizma) (Sigma Aldrich, Italy) 0.1 M, pH 7.4) at a final concentration of 250 µg/mL, according to the protocol described by Shi et al. [14]. Specifically, 5 mg of the samples were kept immersed in 20 mL of buffer up to 14 days at 37 °C in an orbital shaker Excella E24, Eppendorf with an agitation rate of 150 rpm. At each predefined time point (3 h, 24 h, 3 days, 7 days and 14 days) the suspensions were centrifuged for 5 min at 10.000 rpm (Hermle Labortechnik Z326), half of the supernatant was collected and replaced by the same amount of fresh buffer. Each experiment was carried out in triplicate and results are reported and mean ± standard deviation. The concentration of Cu ions was measured by Inductively Coupled Plasma Atomic Emission Spectrometry Technique (ICP-AES) (ICP-MS, Thermoscientific, ICAP Q), after appropriate dilutions.

2.3. Synthesis of Poloxamer-based poly(ether urethane)

2.3.1. Materials

Poloxamer 407 (P407) (PEO-PPO-PEO triblock copolymer, M_n = 12,600 Da, 70% w/w PEO), 1,6-hexamethylene diisocyanate (HDI), dibutyltin dilaurate (DBTDL) and 1,4-cyclohexanedimethanol (CDM) were purchased from Sigma Aldrich (Italy). Before use, with the final aim of removing residual water from the reagents, P407 was dried under reduced pressure at 100 °C for 8 h and then cooled down at 40 °C under vacuum, HDI was distilled under reduced pressure and CDM was kept at room temperature under vacuum in a desiccator. Anhydrous 1–2 dichloroethane (DCE) was prepared by pouring the solvent over activated molecular sieves (3 Å, Sigma Aldrich, Italy) under nitrogen atmosphere overnight. All solvents were purchased from Sigma Aldrich (Italy) in analytical grade.

2.3.2. Synthesis protocol

P407-based PEU was synthesized via a two-step procedure in nitrogen atmosphere, according to the protocol recently published by Boffito et al. [18]. Briefly, P407 was first solubilized in DCE at 20% w/v concentration and equilibrated at 80 °C. HDI was then added at 2:1 molar ratio with respect to P407 and the prepolymerization reaction proceeded for 2.5 h after addition of catalytic amount of DBTDL (0.1% w/w with respect to P407). At the end of the first step, the reaction mixture was equilibrated at 60 °C and the isocyanate-terminated prepolymer was chain extended by adding CDM (3% w/v in DCE) at 1:1 molar ratio with respect to P407. After 1.5 h, the system was cooled down at room temperature and anhydrous methanol was added to stop the reaction. The polymer was then collected by precipitation in petroleum ether (4:1 vol ratio with respect to DCE reaction volume) and purified by dissolution in DCE at 20% w/v followed by precipitation in a mixture of diethyl ether and methanol (98:2 v:v) at 5:1 vol ratio with respect to DCE. Finally, the polymer was collected by centrifugation (Hettich, MIKRO 220R) at 0 °C, 6000 rpm for 20 min, and dried overnight at room temperature under a fume hood.

Hereafter, the synthesized PEU will be referred to as CHP407, where C identifies the chain extender 1,4-cyclohexanedimethanol, H stands for 1,6-hexamethylene diisocyanate and P407 refers to the macrodiol Poloxamer 407.

2.4. Chemical characterization of CHP407

2.4.1. Attenuated Total Reflectance Fourier Transform Infrared (ATR-FTIR) Spectroscopy

Both P407 and CHP407 were characterized by Attenuated Total Reflectance Fourier Transform Infrared (ATR-FTIR) Spectroscopy using a Perkin Elmer Spectrum 100 equipped with an ATR accessory (UATR KRSS) with diamond crystal. The spectra resulted from 16 scans in the spectral range from 4000 to 600 cm^{-1} with a resolution of 4 cm^{-1}. The

analysis were conducted at room temperature and analyzed using the Perkin Elmer Spectrum software.

2.4.2. Size Exclusion Chromatography (SEC)

CHP407 molecular weight distribution was evaluated through an Agilent Technologies 1200 Series (CA, USA) Size Exclusion Chromatography (SEC) equipped with a Refractive Index (RI) detector and two Waters Styragel columns (HR2 and HR4) conditioned at 35 °C, and using tetrahydrofuran (THF, CHROMASOLV Plus, inhibitor-free, for HPLC, 99.9%, Sigma Aldrich, Italy) as mobile phase. Number average molecular weight (M_n) and polydispersity index (D) were measured starting from a calibration curve based on polystyrene standards with peak molecular weight (M_p) in the range 740–180,000 Da using the Agilent ChemStation software. Before analysis, CHP407 powder was dissolved in THF at 2 mg/mL concentration and filtered through a 0.45 µm syringe filter (Whatman).

2.5. Preparation of CHP407-based hydrogels loaded with Cu-MBGs

MBG_Cu 2%_SG and MBG_Cu 2%_SD were loaded in CHP407-based hydrogel with a final particle and PEU concentration of 20 mg/mL and 15% w/v, respectively. PEU concentration was kept at 15% w/v based on our previously published data on the behaviour of aqueous solutions of a PEU with similar building blocks [18]. In order to load CHP407-based hydrogels, a Cu-MBG suspension was first prepared at 100 mg/mL concentration and sonicated (Sonics, Vibracells) with a 20% amplitude for 3 min to improve particle dispersion. Subsequently, a predefined volume of particle suspension was added to CHP407-based solutions previously prepared at higher concentration to reach at the end the requested PEU and particle concentration in the hydrogel. CHP407-based solutions were prepared by powder solubilisation in physiological saline solution (0.9% NaCl) at 5 °C overnight to avoid micellization and/or gelation phenomena that would prevent complete polymer dissolution. For the same reason, particle suspension addition was conducted in a water bath maintained at 5 °C. Each sample was mixed with a Vortex stirrer (Argo LAB Mix) for 30 s to homogeneously disperse the particles inside the hydrogel and stored in the gel state in an incubator (Memmert IF75) at 37 °C to avoid potential particle sedimentation. Before any characterization requiring the system in the sol state, the gels were put in a water bath at 5 °C for 3 min to allow the gel-to-sol transition. Hereafter, CHP407-based sol-gel systems loaded with Cu-MBG particles will be referred to with the acronym CHP407_15%w/v_WW, where WW identifies the Cu-MBG synthesis route (SD or SG). Sol-gel systems not-loaded with mesoporous particles were also prepared and used as control (acronym CHP407_15%w/v).

2.6. Characterization of CHP407-based hydrogels

2.6.1. Tube inverting test

Tube inverting test was carried out to qualitatively determine the sol-to-gel transition temperature. Each sol-gel system (1 mL) was prepared in a sample container (Savatec, Italy) with an inner diameter of 17 mm according to the previously described protocol and subjected to a step-by-step temperature increase within the range 5–70 °C. In each step, the samples were subjected to a temperature increase of 1 ± 0.1 °C, followed by temperature maintenance for 5 min and inversion for 30 s for the visual inspection of the sample sol/gel state. Conditions of sol and gel were defined as "flow liquid sol" and "no flow solid gel" within the 30 s of inversion, respectively.

2.6.2. Gelation time at 37 °C

Gelation time tests were conducted to establish the requested time to reach a complete transition from the sol to the gel state in physiological conditions, i.e. at 37 °C. Samples (1 mL) were prepared in sample containers (Savatec, Italy) with an inner diameter of 17 mm according to the previously described protocol and incubated in an incubator (Memmert IF75) previously equilibrated at 37 °C. At predefined time points of 1, 2, 3, 4, 5, 6, 7, 8, 9 and 10 min the samples were inverted for 30 s for the visual inspection of their sol/gel state. Conditions of sol and gel were defined as in the tube inverting test. At each time point, the samples were equilibrated at 4 °C for 8 min before incubation at 37 °C to ensure that all the systems were in the sol state at the beginning of the test.

2.6.3. Hydrogel injectability

Injectability of CHP407-based sol-gel systems loaded with Cu-MBG particles was tested using a 5 mL plastic syringe through three needles differing for their internal diameter, G22 (diameter 0.64 mm), G18 (diameter 1.02 mm) and G14 (diameter 1.63 mm). Injectability was tested at three different temperatures (5, 25 and 37 °C) by three potential users. Before the test, the sol-gel systems were left at each tested temperature for 25 min to reach thermal stability and system equilibration in the sol, biphasic or gel state.

2.6.4. Hydrogel stability and swelling

Swelling and stability tests were carried out on CHP407-based hydrogels (2 mL) not-loaded and loaded with MBG_Cu 2%_SD and MBG_Cu 2%_SG particles. The prepared samples were weighed (W_i) and incubated at 37 °C for 15 min to allow the complete transition from the sol to the gel state before the beginning of the test. After gelation, 2 mL of Tris HCl buffer solution previously equilibrated at 37 °C were added to each sample. At predefined time steps (3h, 24 h, 3 days, 7 days, 14 days) three samples were taken from the incubator and weighted (W_f) once removed the residual buffer to quantify their absorption ability (Swelling%), while the incubation medium of all other samples incubated at 37 °C was refreshed with Tris HCl (equilibrated at 37 °C prior to addition). Then, the samples were freeze-dried (Martin Christ ALPHA 2–4 LSC, Germany) and weighted again ($W_{freeze\text{-}dried_f}$) to investigate their weight loss (Weight loss%). Control samples (not incubated in buffer solutions) were also freeze-dried and weighed ($W_{freeze\ dried_i}$). Buffer absorption and system stability were estimated according to the following equations:

$$\text{Swelling\%} = \frac{(w_f - w_i)}{w_f} \times 100 \tag{1}$$

$$\text{Weight loss\%} = \frac{(w_{freeze-dried,i} - w_{freeze-dried,f})}{w_{freeze-dried,i}} \times 100 \tag{2}$$

Results are reported as mean ± standard deviation.

At each time point, the morphology of the freeze-dried CHP407 hydrogels loaded with both MBG_Cu 2%_SD and MBG_Cu 2%_SG particles was analyzed by FE-SEM microscopy using a Philips 525 M instrument.

2.6.5. Evaluation of Cu ion release from CHP407 hydrogels loaded with Cu-MBGs

Cu ion release was evaluated from CHP407 hydrogels (2 mL) loaded with both MBG_Cu 2%_SD and MBG_Cu 2%_SG particles. The prepared samples were first incubated at 37 °C for 15 min to allow the complete transition from the sol to the gel state before the beginning of the test. After gelation, 2 mL of Tris HCl previously equilibrated at 37 °C were added to each sample. At predefined time steps (3h, 24 h, 3 days, 7 days, 14 days) the supernatant was refreshed, while the collected volume was centrifuged for 15 min at 6.000 rpm (Hettich, MIKRO 220R) and analyzed by ICP-AES after appropriate dilutions to measure the concentration of released Cu ions. Analyses were conducted in triplicate and results are reported as mean ± standard deviation.

2.7. Statistical analysis

Statistical analysis was performed using GraphPad Prism version 5.00 for Windows (GraphPad Software, La Jolla, CA, USA;

www.graphpad.com). Two-way ANOVA analysis followed by Bonferroni's multiple comparison test was used to compare results. The statistical significance of each comparison was assessed as reported by Boffito et al. [18].

3. Results and discussion

3.1. Cu-MBG characterization

3.1.1. Morphological and structural characterization

FE-SEM images of MBG_Cu 2%_SG (Fig. 1A) showed particles with a uniform spherical morphology, with size ranging between 150 and 200 nm. EDS mapping analysis revealed a homogeneous distribution of silicon (yellow) and calcium (red) throughout the analyzed particles (Fig. 1B), at variance the analysis of copper was not reliable due to presence of the element in the sample holder. EDS spectrum of the powder dispersed on carbon tape (Fig. 1C) confirmed the incorporation of copper inside the framework, with a Cu/Si molar ratio (as average of three measurements) in fair agreement with the nominal ratio.

MBG_Cu 2%_SD, as shown in Fig. 2A, consists of microspheres with size mostly in the range of 1–5 µm, showing silicon (yellow), calcium (green) and copper (light blue) homogeneously distributed into the framework, as revealed by the compositional mapping EDS analysis carried out on a single sphere (Fig. 2B). EDS spectrum of the powder supported on the carbon-based tape revealed the incorporation of copper with a molar concentration very close to the nominal ratio (Fig. 2C).

Wide-angle XRD (Fig. S1) confirmed that copper did not form segregated oxide clusters after calcination treatment, as assessed by the absence of crystalline oxide-based phases.

The N_2 adsorption-desorption isotherms confirmed the mesoporous structure of both copper-containing MBGs (Fig. 3A). The type IV isotherm curve of MBG_Cu 2%_SG showed a well-defined step around 0.4 (P/P_0), indicative of the filling of uniform mesopores. Related DFT pore size distribution (Fig. 3B) confirmed the presence of uniform mesopores with a mean diameter centred at around 4 nm. The BET specific surface area (SSA) and pore volume (reported in Table 1) resulted remarkably high, slightly lower than those reported for similar systems without copper [38].

The isotherm of the sample obtained by aerosol-assisted procedure also confirmed its mesoporous structure. The isotherm (Fig. 3C) is a IV type curve, with H1 hysteresis loop, typical of mesoporous material with pores larger than 4 nm. The pore size distribution showed multi-sized pores with broad distribution, ranging between 8 and 11 nm (Fig. 3D). The specific surface area of MBG_Cu 2%_SD, although lower than the one shown by MBG_Cu 2%_SG, is still very high compared to values typical of not-templated sol-gel glasses (few $m^2 g^{-1}$), which confers an high reactivity to MBGs in the biological environment [5].

3.1.2. Bioactive behaviour of Cu_MBGs

The remarkable bioactivity of MBG_Cu 2%_SG and MBG_Cu 2%_SD when soaked in SBF was clearly revealed by FE-SEM observations. After only 1 day of soaking, the particles started to be covered by a rough layer of globular agglomerates of Ca-deficient hydroxyapatite (HA) phase (Ca/P = 1.51), as shown by EDS analysis (data not shown). After 14 days, MBG particles were almost fully covered by a compact layer of needle-like nanocrystals, composed by calcium and phosphorus. Fig. 4 shows MBG_Cu 2%_SD after soaking for 14 days. EDS analysis performed on powders evidenced a Ca/P ratio of 1.7, typical of hydroxyapatite [39,40].

XRD analysis performed on the MBG particles after the bioactivity test confirmed the formation of crystalline hydroxyapatite: marked peaks appeared at 25.68° and 31.99° (2ϑ value) and other less intense reflections at 39.85°, 46.53° and 49.36° (2ϑ value) matched by hydroxyapatite reference (00-001-1008).

3.1.3. Copper ion release from Cu-MBGs

The ionic concentration (ppm) of Cu^{2+} species from MBG_Cu 2%_SG powder in Tris HCl medium is reported in Fig. 5: almost the total amount of incorporated copper was released within the first 3 h of incubation with a final released concentration of about 4.7 ppm. On the other hand, the release profile from MBG_Cu 2%_SD particles showed a less pronounced burst effect in the first 3 h compared to MBG_Cu 2%_SG, followed by a sustained release of copper ions overtime. The observed release kinetics suggested that the diffusion of Cu^{2+} out of the mesopores is probably hindered or even blocked after the first hours (2–3 h) of incubation. A similar release profile has been already observed from silica-based mesoporous spheres [41] and was ascribed to the progressive occlusion of mesopores due to the dissolution of the silica framework and its re-precipitation as silica gel at the pores mouth [42,43]. The final concentration of released copper species from MBG_Cu 2%_SD was about 2.5 ppm, lower than that found for MBG_Cu 2%_SG, and corresponding to approximately the 60% of incorporated copper, suggesting the presence of a residual amount of copper into the MBG framework or re-precipitation phenomena. The faster ion release kinetics shown for MBG_Cu 2%_SG particles can be ascribed to the remarkably higher surface area and the lower particle size (short diffusion paths), which allow fast ion diffusion inside the porous structure. Furthermore, as MBG_Cu 2%_SD particles are produced by an aerosol-assisted spray-drying process, where a rapid evaporation of the solvent takes place, the resulting powder is expected to show a less condensed framework compared to MBG_Cu 2%_SG and thus much higher reactivity toward surface dissolution/re-precipitation reactions.

3.2. Chemical characterization of CHP407

The success of CHP407 synthesis was assessed by ATR-FTIR spectroscopy, as shown in Fig. 6, which compares the ATR-FTIR spectra of the starting Poloxamer 407 and the as synthesized CHP407 poly(ether urethane).

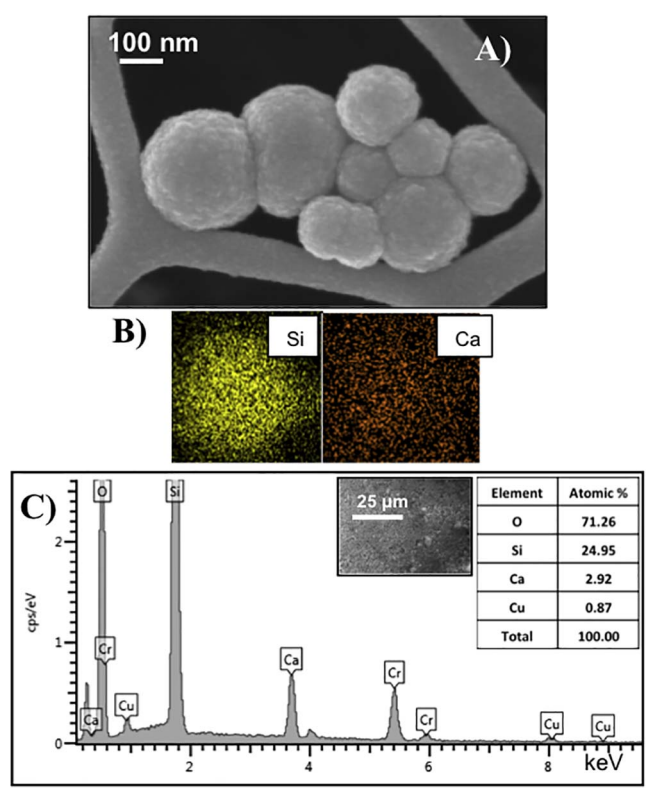

Fig. 1. A) FE-SEM image of MBG_Cu 2%_SG. B) EDS mapping analysis of MBG_Cu 2%_SG. C) EDS spectrum of MBG_Cu 2%_SG (analyzed area of 75 × 50 µm).

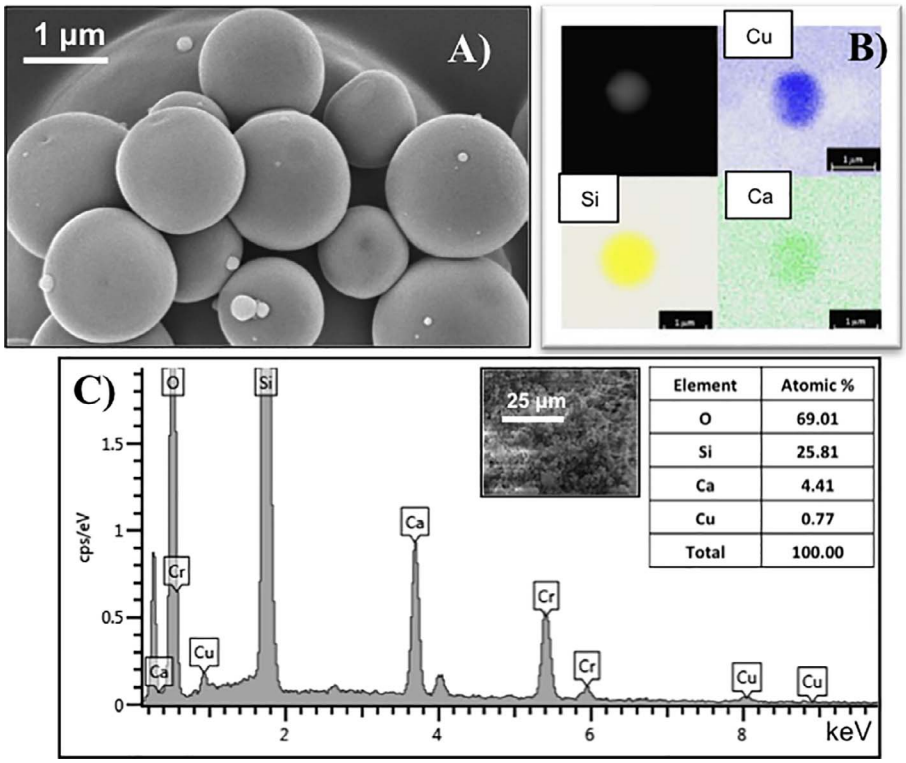

Fig. 2. A) FE-SEM image of MBG_Cu 2%_SD. B) EDS mapping analysis of MBG_Cu 2%_SD single particle. C) EDS spectrum of MBG_Cu 2%_SD (analyzed area of 75 × 50 µm).

The analysis of CHP407 ATR-FTIR spectrum proved the successful synthesis of a poly(ether urethane) containing Poloxamer 407 building blocks, as demonstrated by the presence of the absorption peaks at 2880 and 1099 cm^{-1}, that can be ascribed to the stretching vibration of CH_2 and C–O–C groups, respectively. The successful synthesis of CHP407 was assessed by the appearance of new bands that can be ascribed to the formation of urethane bonds. In detail, the peaks at 1720 and 1530 cm^{-1} can be attributed to the stretching vibration of carbonyl groups (C═O) (amide I) and the bending vibration of N—H bonds (amide II), respectively. The newly formed urethane and amide groups also showed absorption at 3341 cm^{-1}, ascribed to N—H stretching. The absence of an absorption peak at 2200 cm^{-1} due to unreacted diisocyanates proved the complete conversion of the monomers.

Polyurethane average numeral molecular weight (M_n) obtained by SEC was in the range of 50,000–60,000 Da. The low polydispersity index (D) of the polyurethane (1.3) indicates a narrow distribution of the molecular weight and thus a good control over the polymerization process.

Table 1
Structural features of MBG_Cu 2%_SG and MBG_Cu 2%_SD.

Samples	SSA_{BET} ($m^2 g^{-1}$)	Pore Volume ($cm^3 g^{-1}$)	DFT Pore Size (nm)
MBG_Cu 2%_SG	740	0.15	4
MBG_Cu 2%_SD	226	0.05	8–11 nm

3.3. Characterization of CHP407 hydrogels loaded with Cu-MBGs

MBG_Cu 2%_SG and MBG_Cu 2%_SD particles were loaded in 15%

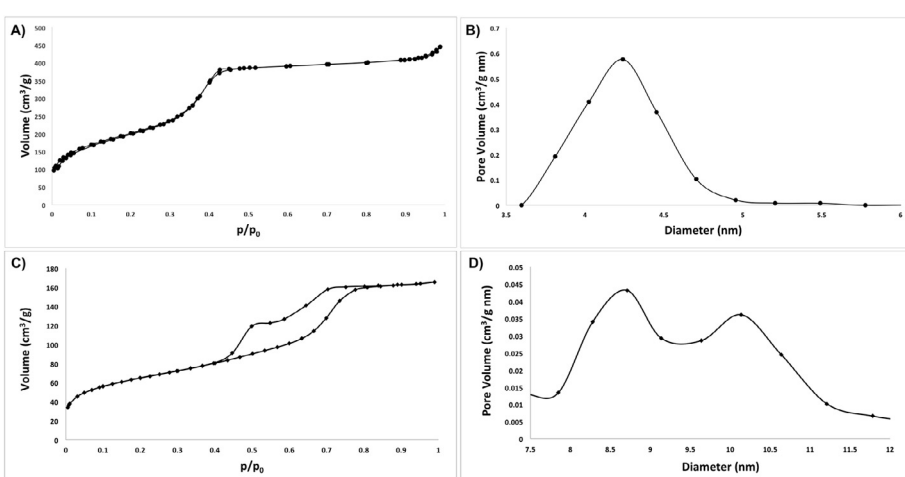

Fig. 3. A) N_2 adsorption-desorption isotherm of MBG_Cu 2%_SG. B) DFT pore size distribution of MBG_Cu 2%_SG. C) N_2 adsorption-desorption isotherm of MBG_Cu 2%_SD. D) DFT pore size distribution of MBG_Cu 2%_SD.

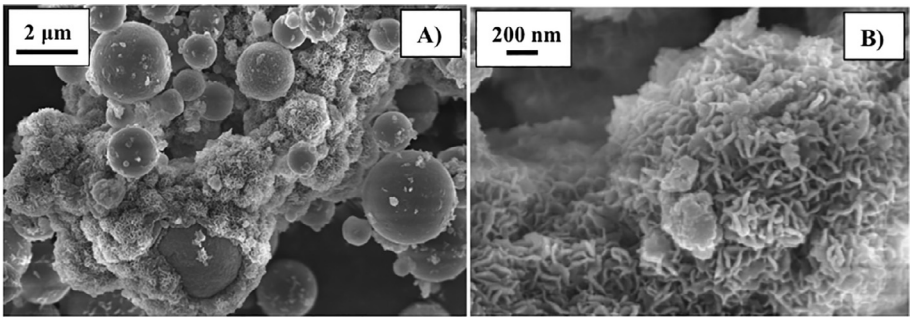

Fig. 4. FE-SEM of MBG_Cu 2%_SD after 14 day of soaking in SBF (A) and high magnification of A image (B).

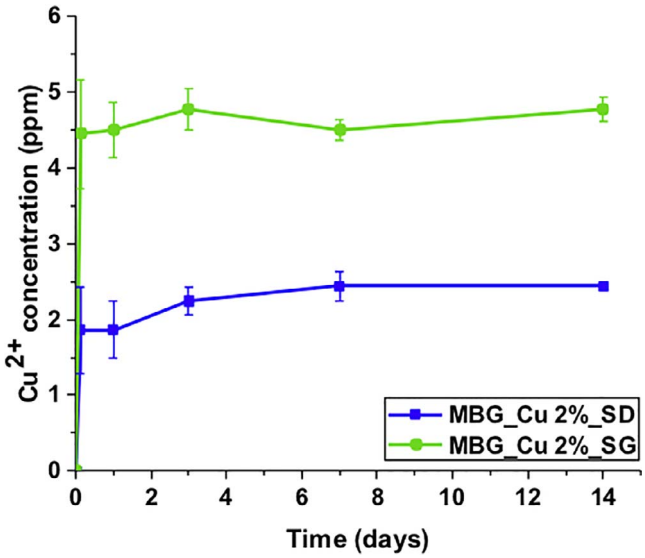

Fig. 5. Cu^{2+} release profiles in Tris HCl from MBG_Cu 2%_SG and MBG_Cu 2%_SD.

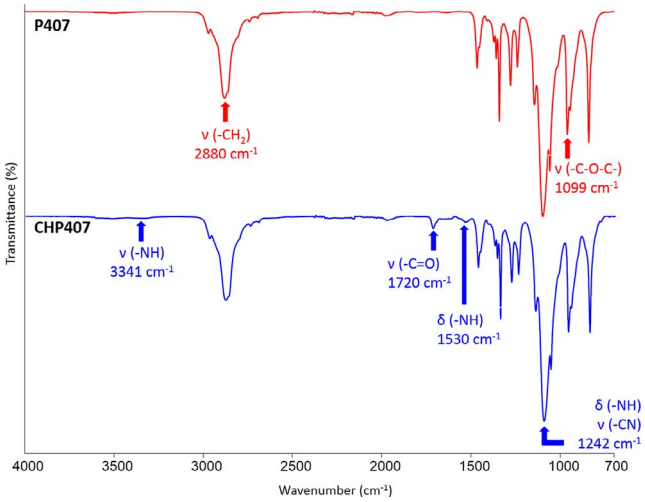

Fig. 6. ATR-FTIR spectra of Poloxamer 407 (red) and the as synthesized CHP407 poly (ether urethane) (blue). Differences between the spectra that prove the success of the synthesis process are highlighted in blue, while the typical peaks of P407 are evidenced in red. (For interpretation of the references to colour in this figure legend, the reader is referred to the web version of this article.)

w/v concentrated CHP407 aqueous solutions at a final concentration of 20 mg/mL. The newly designed hybrid injectable systems were characterized in terms of their thermosensitivity and gelation kinetics, injectability, stability and swelling in physiological conditions, and Cu^{2+} ion release kinetics.

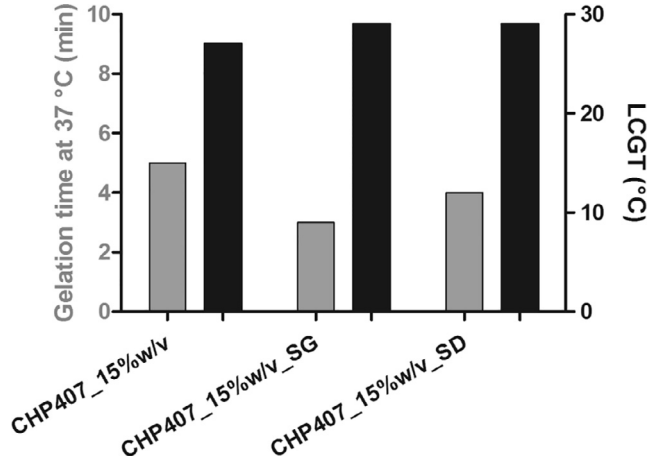

Fig. 7. Lower critical gelation temperature (LCGT) values (black) and gelation time in physiological conditions (37 °C) (grey) of CHP407_15%w/v and CHP407 sol-gel systems with 15% w/v PEU concentration loaded with MBG_Cu 2%_SG and MBG_Cu 2%_SD particles at 20 mg/mL (CHP407_15%w/v_SG and CHP407_15%w/v_SD) obtained by tube inverting test. Error: ± 0.5 °C for LCGT values, ± 30 s for gelation time values.

3.3.1. Lower critical gelation temperature and gelation time in physiological conditions

Tube inverting and gelation time tests allowed the investigation of the effects of particle loading on the gelation of CHP407-based sol-gel systems. Fig. 7 reports Lower Critical Gelation Temperature (LCGT) values and gelation time in physiological conditions (37 °C) of CHP407_15%w/v sol-gel systems loaded and not-loaded with both MBG_Cu 2%_SG and MBG_Cu 2%_SD at 20 mg/mL concentration.

Irrespective of the type of incorporated particles (SG or SD), LCGT values tended to slighly increase upon Cu-MBG loading in the hybrid sol-gel systems (27 °C for CHP407_15%w/v, 29 °C for both CHP407_15%w/v_SD and CHP407_15%w/v_SG). This behaviour suggests that, most likely, mesoporous particles hinder or slow down the kinetics of micelle formation and packing into a fully developed gel with increasing temperature. Similarly to the not-loaded control sample (CHP407_15%w/v), loaded sol-gel systems did not show a gel-to-sol transition up to 70 °C. The trend of gelation time at 37 °C was opposite to that observed for LCGTs. In fact, gelation time at 37 °C slighly decreased upon Cu-MBG particles loading, irrespective of the synthesis route used to prepare them (from 5 min for CHP407_15%w/v to 3 and 4 min for CHP407_15%w/v_SG and CHP407_15%w/v_SD, respectively). The decrease in gelation time in physiological conditions can be correlated to an increase in the viscosity of the systems upon particle incorporation, as typical of colloidal systems. Although the kinetics of gel formation and development slow down, as suggested by the tube inverting test results, an increase in the viscosity of the systems can account for a decrease in gelation time in isothermal conditions, being the conditions of sol and gel defined as “flow liquid sol” and “no flow solid gel” within 30 s of tube inversion, respectively. For what concerns the

influence of particle type on gelation time in physiological conditions, MBG_Cu 2%_SG-loaded hydrogels exhibited a faster gelation than MBG_Cu 2%_SD-loaded systems. This behaviour can be correlated to the different size and size distribution of MBG_Cu 2%_SG compared to MBG_Cu 2%_SD. As MBG_Cu 2%_SG particles show smaller particle size and narrower size distribution, on equal suspension concentration, higher amount of particles and better dispersion inside CHP407-based hydrogel is expected compared to MBG_Cu 2%_SD, thus inducing a higher viscosity of the final hybrid formulation.

3.3.2. Qualitative evaluation of hydrogel injectability

MBG_Cu 2%_SG- and MBG_Cu 2%_SD-loaded CHP407 sol-gel systems with 15% w/v PEU concentration and 20 mg/mL particle content were characterized in terms of their injectability at different temperatures (5, 25 and 37 °C) through different needles (G22, G18, G14) (Table 2).

At 5 °C, all the prepared samples were in the sol phase and easy injectable through all needles. With increasing temperature, irrespective of the presence of Cu-MBG particles, all CHP407 (15%w/v) solutions underwent a transition from the sol to the gel state. As a consequence of this transition, viscosity increased leading to the impossibility to inject the gels through G22 needle at both 25 and 37 °C. On the contrary, all the samples turned out to be still injectable through the largest tested needle, i.e. G14. For what concerns G18 needle, the gel CHP407 (15%w/v) loaded with MBG_Cu 2%_SG was not injectable at both 25 and 37 °C, while the control gel (CHP407_15%w/v) and the sample loaded with MBG_Cu 2%_SD retained their injectability. This different behaviour can be ascribed to the higher viscosity and faster gel formation and development of CHP407_15%w/v_SG sol-gel systems compared to both MBG_Cu 2%_SD-loaded hydrogel and not-loaded CHP407_15%w/v, as also suggested by tube inverting and gelation time tests results.

The tested range of needle diameters (G22-G14) and gel storage conditions (5, 25 and 37 °C) open the way to different potential applications of the designed hybrid sol-gel systems, such as intramuscular injection (suggested needles in the range G21-G23), intra-bone injection (G13 needle is usually used for percutaneous vertebroplasty), topical application on infected skin wounds (no particular needs to be addressed).

3.3.3. Hydrogel stability and swelling

CHP407-based gels with a 15% w/v PEU concentration and loaded with MBG_Cu 2%_SG and MBG_Cu 2%_SD particles at 20 mg/mL were characterized in terms of their swelling behaviour and stability in aqueous environment in the presence of a buffer solution at pH 7.4 at 37 °C. Not-loaded CHP407-based gels with the same polymer concentration (CHP407_15%w/v) were also analyzed to assess the influence of particle loading on these properties. Fig. 8 reports the percentage of swelling (Fig. 8A) and dissolution (Fig. 8B) of loaded and not-loaded CHP407 gels at different time points, evaluated according to the equations defined in paragraph 2.6.4.

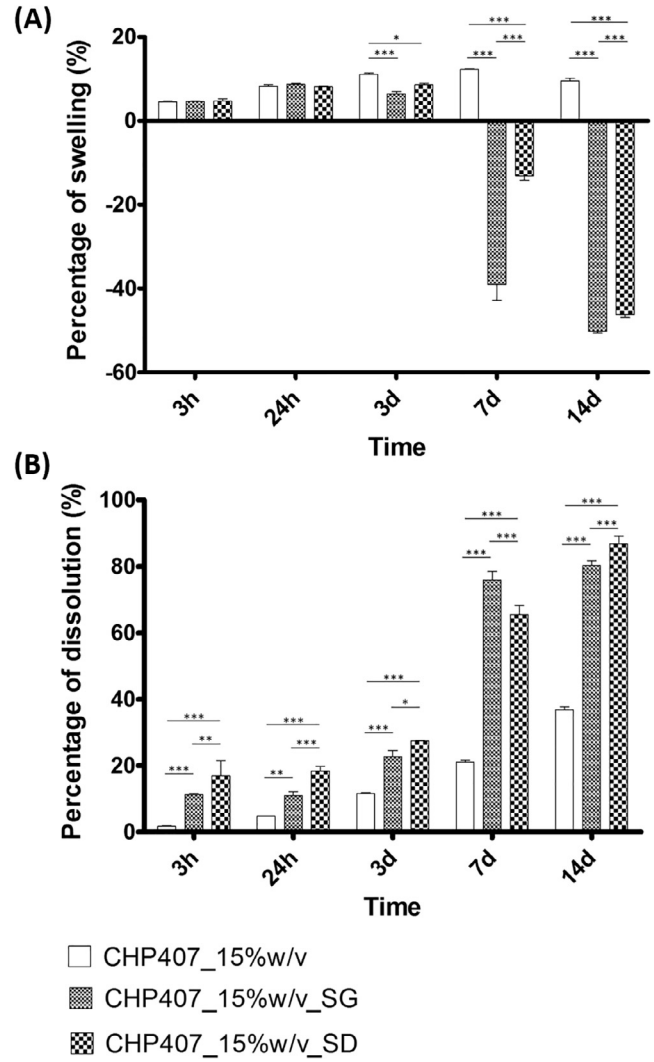

Fig. 8. (A) Buffer (pH 7.4) absorption and (B) dissolution percentages as a function of time of CHP407_15%w/v, CHP407_15%w/v_SG and CHP407_15%w/v_SD gels.

Up to 24 h of incubation time, loaded gels showed a degree of swelling similar to not-loaded CHP407_15%w/v gels (approx. 4.5%). However, after 3 days incubation, loaded gels showed a significant decrease in swelling percentage compared to not-loaded CHP407_15% w/v (swelling percentage of 11.0 ± 0.3%), suggesting that dissolution phenomena became more relevant than swelling for Cu-MBG loaded gels (8.6 ± 0.3% and 6.4 ± 0.6% for CHP407_15%w/v_SD and CHP407_15%w/v_SG, respectively). On day 7, CHP407_15%w/v_SG and CHP407_15%w/v_SD showed negative swelling data, which means that dissolution had totally overstepped swelling phenomena. Indeed,

Table 2
Injectability of CHP407_15%w/v sol-gel systems loaded and not-loaded with MBG_Cu 2%_SG and MBG_Cu 2%_SD at 20 mg/mL concentration evaluated at different temperatures (5, 25 and 37 °C) through different needles (G22, G18, G14). Codes: X – not injectable; V – injectable; d_{int} – internal diameter.

		CHP407_15%w/v	CHP407_15%w/v_SG	CHP407_15%w/v_SD
5 °C	G22 (d_{int} = 0.64 mm)	*V*	*V*	*V*
	G18 (d_{int} = 1.02 mm)	*V*	*V*	*V*
	G14 (d_{int} = 1.63 mm)	*V*	*V*	*V*
25 °C	G22 (d_{int} = 0.64 mm)	*X*	*X*	*X*
	G18 (d_{int} = 1.02 mm)	*V*	*X*	*V*
	G14 (d_{int} = 1.63 mm)	*V*	*V*	*V*
37 °C	G22 (d_{int} = 0.64 mm)	*X*	*X*	*X*
	G18 (d_{int} = 1.02 mm)	*V*	*X*	*V*
	G14 (d_{int} = 1.63 mm)	*V*	*V*	*V*

loaded gels were almost completely dissolved after 7 days of incubation (dissolution of 65.4 ± 2.8% and 76.0 ± 2.4% for CHP407_15%w/v_SD and CHP407_15%w/v_SG, respectively), while the not-loaded CHP407_15%w/v gels showed only a partial dissolution of 21.1 ± 0.6%. After 14 days of incubation in aqueous environment at 37 °C, the swelling percentage of CHP407_15%w/v gels slightly decreased with respect to 7 days (12.3 ± 0.2% *vs* 9.6 ± 0.6%, not significant difference), suggesting that, differently from loaded samples, dissolution started to prevail over absorption after 7 days incubation time. The dissolution degree increased over time for all the analyzed samples and it was significantly more pronounced in MBG particles-loaded gels with respect to not-loaded CHP407_15%w/v at each time points, suggesting that particle incorporation significantly affects the stability of the resulting hybrid systems in an aqueous environment, irrespective of their morphological features.

The morphology of hybrid hydrogels was also characterized through FE-SEM observation (Fig. 9) before soaking in Tris HCl buffer (time 0) and at different time points (24 h and 7 days). No images were recorded at 14 days incubation time as the hybrid samples were completely dissolved at this time point, as shown also in Fig. 8. FE-SEM images of both CHP407_15%w/v_SG and CHP407_15%w/v_SD at time 0 (prior to incubation) revealed a good and homogeneous particle dispersion into the hydrogel network with small aggregates composed by few particles (from 2 to 5 particles). FE-SEM analysis showed no significant changes in the morphology of the hybrid systems after 24 h and 7 days immersion in Tris HCl solution. Furthermore, the size of MBG particles embedded into the hydrogels was not significantly affected by the immersion into an aqueous medium.

3.3.4. Evaluation of Cu ion release from CHP407 hydrogels loaded with Cu-MBGs

Release properties of Cu-MBGs embedded in CHP407 hydrogel have been studied by soaking the hybrid gels in Tris HCl previously equilibrated at 37 °C. At predefined time steps (3 h, 24 h, 3 days, 7 days, 14 days) the supernatants were collected and Cu^{2+} ion concentration measured. Fig. 10 reports the release profiles obtained for CHP407_15%w/v_SG and CHP407_15%w/v_SD. At variance with the release behaviour of MBG_Cu 2%_SG particles, where a pronounced initial burst effect was observed, CHP407_15%w/v_SG showed a sustained release of Cu^{2+} species with a slower kinetics. These data confirm that particles are accessible to the soaking medium, although incorporated into the hydrogel, and able to deliver Cu^{2+} species through ion-exchange reactions. Copper was successfully released also from CHP407_15%w/v_SD, although the final released concentration after 14 days was lower than that measured for CHP407_15%w/v_SG, in analogy with the released concentrations from MBG particles alone. This seems to suggest that incorporated particles retain their release properties and reactivity despite their embedding into the thermosensitive sol-gel systems, which is a crucial aspect in view of the final application. Furthermore, the amounts of copper released from the hybrid formulations, normalized

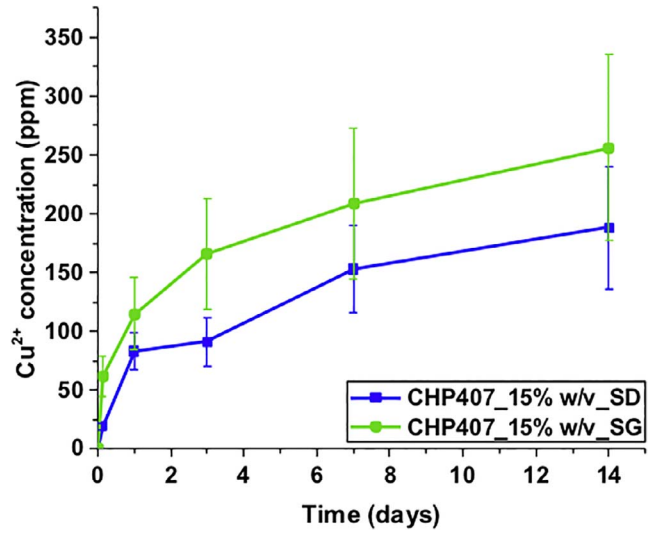

Fig. 10. Cu^{2+} release profiles in Tris HCl at 37 °C from CHP407_15%w/v_SG and CHP407_15%w/v_SD.

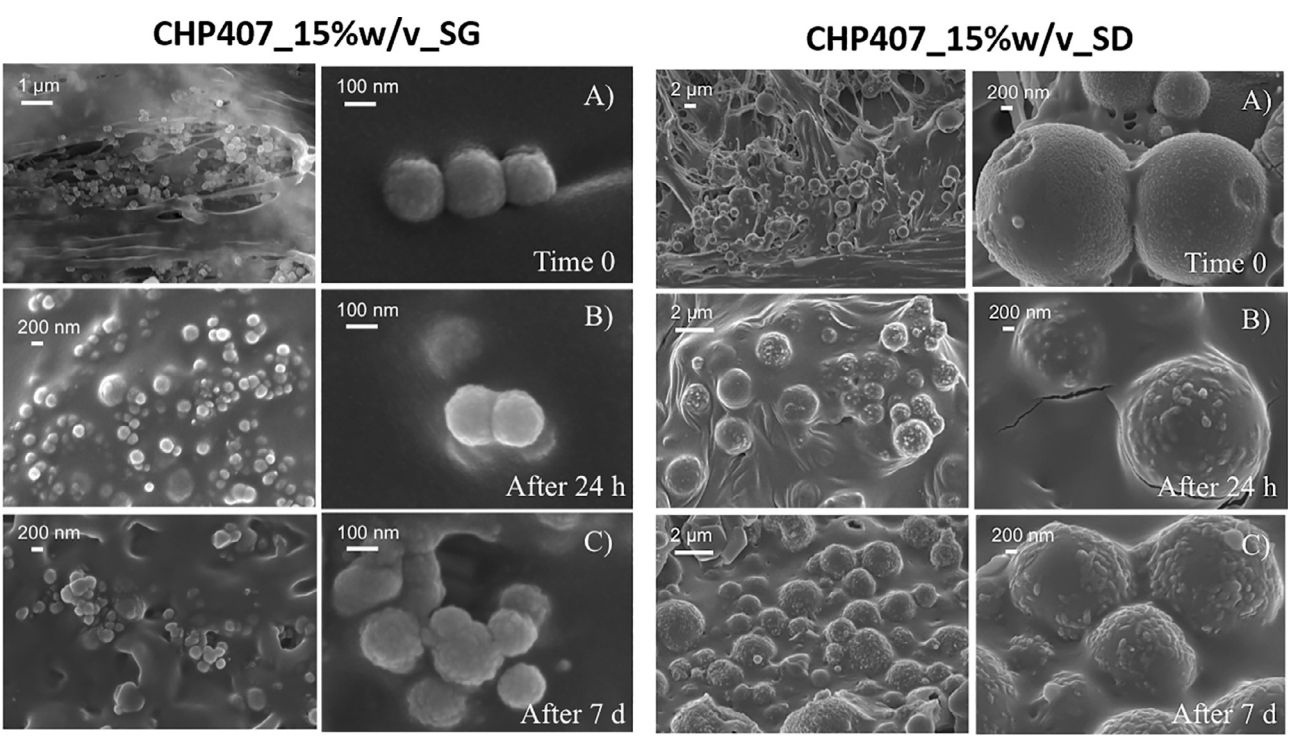

Fig. 9. FE-SEM images of freeze-dried samples of CHP407_15%w/v_SG (on the left) and CHP407_15%w/v_SD (on the right) before soaking in Tris HCl medium (A), after 24 h (B) and 7 days (C) of incubation.

on the amount of releasing powder, are comparable to those obtained from Cu-MBGs alone.

4. Conclusions

In this work, a novel platform of hybrid injectable formulations for *in situ* delivery of therapeutic ions was developed by incorporating copper containing MBG nano- or microspheres into a thermosensitive polyurethane-based hydrogel, able to concentrate and maintain the multifunctional carriers at the pathological site and to guarantee *in situ* and prolonged release of ions/drugs. The composition of the injectable hydrogel was tailored in order to improve gelation kinetics and stability in aqueous environment.

Irrespective of the embedded Cu-MBG size, the designed hybrid formulations showed fast gelation in physiological conditions (a volume of 1 mL undergoes complete sol-to-gel transition within few minutes of incubation at 37 °C) and injectability in a wide range of temperatures through different needles (temperature range 5–37 °C, needles with inner diameter in the range 0.6–1.6 mm). Moreover, although MBG particle incorporation significantly affected the stability of the hybrid hydrogels in aqueous environment, leading to a complete dissolution after 14 days of incubation, the developed hybrid formulations showed the ability to remain *in situ* for several days, thus allowing the release of Cu^{2+} ions with a sustained and prolonged kinetics with respect to Cu-MBG particles as such.

Hence, the herein designed and characterized hybrid platforms show great potential as *in situ* injectable delivery systems of therapeutic ions and/or drugs for the treatment of delayed bone regeneration and wound healing.

Acknowledgement

The activity leading to this research has received funding from H2020-NMP-PILOTS-2015 under grant agreement no. 685872 (MOZART) and by Fondazione CRT under the initiative La Ricerca dei Talenti.

Appendix A. Supplementary data

Supplementary data associated with this article can be found, in the online version, at http://dx.doi.org/10.1016/j.cej.2018.01.073.

References

[1] M. Manzano, M. Vallet-Regí, New developments in ordered mesoporous materials for drug delivery, J. Mater. Chem. 20 (2010) 5593.
[2] J.L. Vivero-Escoto, I.I. Slowing, B.G. Trewyn, V.S.Y. Lin, Mesoporous silica nanoparticles for intracellular controlled drug delivery, Small 6 (2010) 1952–1967.
[3] Z. Li, J.C. Barnes, A. Bosoy, J.F. Stoddart, J.I. Zink, Mesoporous silica nanoparticles in biomedical applications, Chem. Soc. Rev. 41 (2012) 2590–2605.
[4] X. Yan, C. Yu, X. Zhou, J. Tang, D. Zhao, Highly ordered mesoporous bioactive glasses with superior in vitro bone-forming bioactivities, Angew. Chem. – Int. Ed. 43 (2004) 5980–5984.
[5] A. López-Noriega, D. Arcos, I. Izquierdo-Barba, Y. Sakamoto, O. Terasaki, M. Vallet-Regí, Ordered mesoporous bioactive glasses for bone tissue regeneration, Chem. Mater. 18 (2006) 3137–3144.
[6] M. Colilla, Silica- based ceramics: mesoporous silica, in: M. Vallet-Regì (Ed.), Bio-Ceramics with Clinical Applications, John Wiley & Sons Ltd, United Kindom, 2014, pp. 109–151.
[7] C. Wu, J. Chang, Multifunctional mesoporous bioactive glasses for effective delivery of therapeutic ions and drug/growth factors, J. Control. Release 193 (2014) 282–295.
[8] M. Erol-Taygun, K. Zheng, A.R. Boccaccini, Nanoscale bioactive glasses in medical applications, Int. J. Appl. Glas. Sci. 4 (2013) 136–148.
[9] C. Wu, Y. Zhou, M. Xu, P. Han, L. Chen, J. Chang, Y. Xiao, Copper-containing mesoporous bioactive glass scaffolds with multifunctional properties of angiogenesis capacity, osteostimulation and antibacterial activity, Biomaterials 34 (2013) 422–433.
[10] H. Lin, J. Zhang, F. Qu, J. Jiang, P. Jiang, In vitro hydroxyapatite-forming ability and antimicrobial properties of mesoporous bioactive glasses doped with Ti/Ag, J. Nanomater. 2013 (2013).
[11] N. Gargiulo, A.M. Cusano, F. Causa, D. Caputo, P.A. Netti, Silver-containing mesoporous bioactive glass with improved antibacterial properties, J. Mater. Sci. Mater. Med. 24 (2013) 2129–2135.
[12] C. Stähli, M. James-Bhasin, A. Hoppe, A.R. Boccaccini, S.N. Nazhat, Effect of ion release from Cu-doped 45S5 Bioglass® on 3D endothelial cell morphogenesis, Acta Biomater. 19 (2015) 15–22.
[13] S. Zhao, L. Li, H. Wang, Y. Zhang, X. Cheng, N. Zhou, M.N. Rahaman, Z. Liu, W. Huang, C. Zhang, Wound dressings composed of copper-doped borate bioactive glass microfibers stimulate angiogenesis and heal full-thickness skin defects in a rodent model, Biomaterials 53 (2015) 379–391.
[14] M. Shi, Z. Chen, S. Farnaghi, T. Friis, X. Mao, Y. Xiao, C. Wu, Copper-doped mesoporous silica nanospheres, a promising immunomodulatory agent for inducing osteogenesis, Acta Biomater. 30 (2016) 334–344.
[15] A. Bari, N. Bloise, S. Fiorilli, G. Novajra, M. Vallet-Regí, G. Bruni, A. Torres-Pardo, J.M. González-Calbet, L. Visai, C. Vitale-Brovarone, Copper-containing mesoporous bioactive glass nanoparticles as multifunctional agent for bone regeneration, Acta Biomater. 55 (2017) 493–504.
[16] C.P. Silveira, L.M. Apolinàrio, W.J. Fàvaro, A.J. Paula, N. Duràn, Doxorubicin-functionalized silica nanoparticles incorporated into a thermoreversible hydrogel and intraperitoneally administered result in high prostate antitumor activity and reduced cardiotoxicity of doxorubicin, ACS Biomater. Sci. Eng. 2 (2016) 1190–1199.
[17] M. Boffito, P. Sirianni, A.M. Di Rienzo, V. Chiono, Thermosensitive block copolymer hydrogels based on poly(ε-caprolactone) and polyethylene glycol for biomedical applications: state of the art and future perspectives, J. Biomed. Mater. Res. A 1–15 (2014).
[18] M. Boffito, E. Gioffredi, V. Chiono, S. Calzone, E. Ranzato, S. Martinotti, G. Ciardelli, Novel polyurethane-based thermosensitive hydrogels as drug release and tissue engineering platforms: design and in vitro characterization, Polym. Int. 65 (2016) 756–769.
[19] E. Gioffredi, M. Boffito, S. Calzone, S.M. Giannitelli, A. Rainer, M. Trombetta, P. Mozetic, V. Chiono, Pluronic F127 hydrogel characterization and biofabrication in cellularized constructs for tissue engineering applications, Procedia CIRP, 2016, pp. 125–132.
[20] S. Sartori, M. Boffito, P. Serafini, A. Caporale, A. Silvestri, E. Bernardi, M.P. Sassi, F. Boccafoschi, G. Ciardelli, Synthesis and structure-property relationship of polyester-urethanes and their evaluation for the regeneration of contractile tissues, React. Funct. Polym. 73 (2013) 1366–1376.
[21] C. Mattu, M. Boffito, S. Sartori, E. Ranzato, E. Bernardi, M.P. Sassi, A.M. Di Rienzo, G. Ciardelli, Therapeutic nanoparticles from novel multiblock engineered polyesterurethanes, J. Nanoparticle Res. 14 (2012) 1306–1318.
[22] C. Mattu, A. Silvestri, T.R. Wang, M. Boffito, E. Ranzato, C. Cassino, G. Ciofani, G. Ciardelli, Surface-functionalized polyurethane nanoparticles for targeted cancer therapy, Polym. Int. 65 (2016) 770–779.
[23] C. Mattu, R.M. Pabari, M. Boffito, S. Sartori, G. Ciardelli, Z. Ramtoola, Comparative evaluation of novel biodegradable nanoparticles for the drug targeting to breast cancer cells, Eur. J. Pharm. Biopharm. 85 (2013) 463–472.
[24] A. Silvestri, S. Sartori, M. Boffito, C. Mattu, A.M. Di Rienzo, F. Boccafoschi, G. Ciardelli, Biomimetic myocardial patches fabricated with poly(ε -caprolactone) and polyethylene glycol-based polyurethanes, J. Biomed. Mater. Res. – Part B Appl. Biomater. 102 (2014) 1002–1013.
[25] V. Chiono, P. Mozetic, M. Boffito, S. Sartori, E. Gioffredi, A. Silvestri, A. Rainer, S.M. Giannitelli, M. Trombetta, D. Nurzynska, F. Di Meglio, C. Castaldo, R. Miraglia, S. Montagnani, G. Ciardelli, Polyurethane-based scaffolds for myocardial tissue engineering, Interface Focus 4 (2013) 20130045.
[26] M. Boffito, E. Bernardi, S. Sartori, G. Ciardelli, M.P. Sassi, A mechanical characterization of polymer scaffolds and films at the macroscale and nanoscale, J. Biomed. Mater. Res. – Part A 103 (2015) 162–169.
[27] C. Tonda-Turo, M. Boffito, C. Cassino, P. Gentile, G. Ciardelli, Biomimetic polyurethane – based fibrous scaffolds, Mater. Lett. 167 (2016) 9–12.
[28] M.N. Huang, Y.L. Wang, Y.F. Luo, Biodegradable and bioactive porous polyurethanes scaffolds for bone tissue engineering, J. Biomed. Sci. Eng. 2 (2009) 36–40.
[29] K. Gorna, S. Polowinski, S. Gogolewski, Synthesis and characterization of biodegradable poly(ε-caprolactone urethane)s. I. Effect of the polyol molecular weight, catalyst, and chain extender on the molecular and physical characteristics, J. Polym. Sci. Part A Polym. Chem. 40 (2002) 156–170.
[30] K. Gorna, S. Gogolewski, Biodegradable polyurethanes for implants. II. In vitro degradation and calcification of materials from poly(ε-caprolactone)-poly(ethylene oxide) diols and various chain extenders, J. Biomed. Mater. Res. 60 (2002) 592–606.
[31] J.M. Page, E.M. Prieto, J.E. Dumas, K.J. Zienkiewicz, J.C. Wenke, P. Brown-Baer, S.A. Guelcher, Biocompatibility and chemical reaction kinetics of injectable, settable polyurethane/allograft bone biocomposites, Acta Biomater. 8 (2012) 4405–4416.
[32] V. Chiono, S. Sartori, A. Rechichi, C. Tonda-Turo, G. Vozzi, F. Vozzi, M. D'Acunto, C. Salvadori, F. Dini, G. Barsotti, F. Carlucci, S. Burchielli, S. Nicolino, C. Audisio, I. Perroteau, P. Giusti, G. Ciardelli, Poly(ester urethane) guides for peripheral nerve regeneration, Macromol. Biosci. 11 (2011) 245–256.
[33] Y. Khan, M.J. Yaszemski, A.G. Mikos, C.T. Laurencin, Tissue engineering of bone: material and matrix considerations, J. Bone Jt. Surgery-American 90 (2008) 36–42.
[34] I.C. Bonzani, R. Adhikari, S. Houshyar, R. Mayadunne, P. Gunatillake, M.M. Stevens, Synthesis of two-component injectable polyurethanes for bone tissue engineering, Biomaterials 28 (2007) 423–433.
[35] C. Wu, J. Chang, W. Fan, Bioactive mesoporous calcium-silicate nanoparticles with excellent mineralization ability, osteostimulation, drug-delivery and antibacterial properties for filling apex roots of teeth, J. Mater. Chem. 22 (2012) 16801–16809.

[36] L. Pontiroli, M. Dadkhah, G. Novajra, I. Tcacencu, S. Fiorilli, C. Vitale-Brovarone, An aerosol-spray-assisted approach to produce mesoporous bioactive glass microspheres under mild acidic aqueous conditions, Mater. Lett. 190 (2017) 111–114.
[37] A.L.B. Maçon, T.B. Kim, E.M. Valliant, K. Goetschius, R.K. Brow, D.E. Day, A. Hoppe, A.R. Boccaccini, I. Yong Kim, C. Ohtsuki, T. Kokubo, A. Osaka, M. Vallet-Regì, D. Arcos, L. Fraile, A.J. Salinas, A.V. Teixeira, Y. Vueva, R.M. Almeida, M. Miola, C. Vitale-Brovarone, E. Vernè, W. Höland, J.R. Jones, A unified in vitro evaluation for apatite-forming ability of bioactive glasses and their variants, J. Mater. Sci. Mater. Med. 26 (2015) 115.
[38] A. El-Fiqi, T.H. Kim, M. Kim, M. Eltohamy, J.E. Won, E.J. Lee, H.W. Kim, Capacity of mesoporous bioactive glass nanoparticles to deliver therapeutic molecules, Nanoscale 4 (2012) 7475–7488.
[39] V. Uskokovic, D.P. Uskokovic, Nanosized hydroxyapatite and other calcium phosphates: chemistry of formation and application as drug and gene delivery agents, J. Biomed. Mater. Res. Part B Appl. Biomater. 96 (B) (2011) 152–191.
[40] K. Lin, C. Wu, J. Chang, Advances in synthesis of calcium phosphate crystals with controlled size and shape, Acta Biomater. 10 (2014) 4071–4102.
[41] R. Mortera, S. Fiorilli, E. Garrone, E. Verné, B. Onida, Pores occlusion in MCM-41 spheres immersed in SBF and the effect on ibuprofen delivery kinetics: a quantitative model, Chem. Eng. J. 156 (2010) 184–192.
[42] P. Li, K. Nakanishi, T. Kokubo, K. de Groot, Induction and morphology of hydroxyapatite, precipitated from metastable simulated body fluids on sol-gel prepared silica, Biomaterials 14 (1993) 963–968.
[43] P. Li, I. Kangasniemi, K. de Groot, T. Kokubo, A.U. Yli-Urpo, Apatite crystallization from metastable calcium phosphate solution on sol-gel-prepared silica, J. Non. Cryst. Solids 168 (1994) 281–286.